Segmentation of speckle images based on level-crossing statistics

Robert H. Sperry and Kevin J. Parker

Department of Electrical Engineering, Rochester Center for Biomedical Ultrasound, University of Rochester, Rochester, New York 14627

Received May 14, 1990; accepted November 5, 1990

When imaging is performed by using a coherent signal, the result is frequently a realization of the stochastic process known as speckle. The information sought from this process is often the mean value of its envelope or intensity at each point in the image plane. When only a single realization of the process is available, ergodicity is required within a sufficiently large region for accurate estimation of the mean. The identification of these regions is the segmentation problem that is addressed. The approach presented clips the speckle image at a constant threshold level and analyzes the resulting bilevel image based on the level-crossing statistics of the speckle process. An analysis of the level-crossing process leads to a decision rule for identifying or segmenting distinct regions of the image based on the sizes of the fades and the excursions in the clipped speckle. The measurement of these sizes is accomplished by using the morphological transformations of opening and closing. This new approach has been applied to computer-generated speckle images and may prove useful in laser, ultrasound, and radar imaging, in which speckle phenomena are manifest.

1. INTRODUCTION

Implicit in our discussion is a model for image formation that produces a stochastic process referred to in the literature as fully developed speckle. The first- and second-order statistical properties of speckle are well known[1] and are closely related to those encountered in the study of Gaussian noise processes in statistical communications.[2] There has been recent interest in the statistical properties of clipped speckle, arising from the reduced computational complexity of working with 1-bit/pixel images.[3,4] To date, the study of clipped speckle has focused on the first- and second-order statistical properties generated by clipping the trajectories $I(x)$ of a speckle process. Throughout this paper when we refer to clipping, we mean hard clipping at a constant threshold level u, defined as

$$I_u(x) = \begin{cases} 1, & I(x) \geq u \\ 0, & I(x) < u \end{cases}. \tag{1}$$

The results that are presented here differ from previous results related to the study of clipped speckle in that our results are based on the level crossings of the envelope of a Gaussian noise processes.[5,6] Furthermore, the inferences being made from the data differ in that we are not attempting to estimate parameters of the unclipped speckle process but are instead segmenting an image based on the distributions of the random variables related to the level crossings, given hypothesized distributions.

Our interest in speckle derives from research in biomedical imaging with ultrasound, for which it is necessary to select homogeneous regions of interest for the estimation of quantitative parameters such as the attenuation or backscattering coefficients of the tissues being imaged.[7] Since ultrasound B scans of tissues such as liver are multiplicatively contaminated with speckle noise, our goal is to segment an image containing several regions differing only in their mean intensities on the basis of that mean.[8,9] Once the images are segmented, the desired quantitative parameters may then be estimated in the regions identified as statistically homogeneous.

The rationale behind our approach can best be demonstrated by using the image of Fig. 1(a), which contains two Rayleigh distributed regions. The Rayleigh distribution

$$p_V(v) = \begin{cases} \dfrac{v}{\psi} \exp\left(-\dfrac{v^2}{2\psi}\right), & v > 0 \\ 0, & \text{otherwise} \end{cases} \tag{2}$$

arises when the envelope of a complex Gaussian process is considered, and its mean is given in terms of the parameter ψ as $\mu = (\pi/2)^{1/2}\psi^{1/2}$. Denote the interior, bright circular region in the image as R_i and the exterior region as R_e, having parameters ψ_i and ψ_e, respectivly. The desired result is the assignment of each point in the image to the appropriate region. If each pixel were independent, an appropriate rule for assigning membership to the regions might be a maximum-likelihood decision rule.[10] The application of this rule to the decision between two Rayleigh distributions of known parameters ψ_i and ψ_e results in clipping the image at the threshold level

$$v \underset{d_i}{\overset{d_e}{\lessgtr}} \left[\frac{2 \ln\left(\dfrac{\psi_i}{\psi_e}\right)}{\dfrac{1}{\psi_i} - \dfrac{1}{\psi_e}} \right]^{1/2}, \tag{3}$$

where the notation reflects that the decision d_i, in which the point is assigned to the region R_i, occurs when v is greater than the right-hand side of the equation and that the decision d_e, in which the point is assigned in the region R_e, occurs when v is less.[11] The application of this rule to the image of Fig. 1(a) yields Fig. 1(b).

The pixels, however, are not independent. Consider the

0740-3232/91/030490-09$05.00

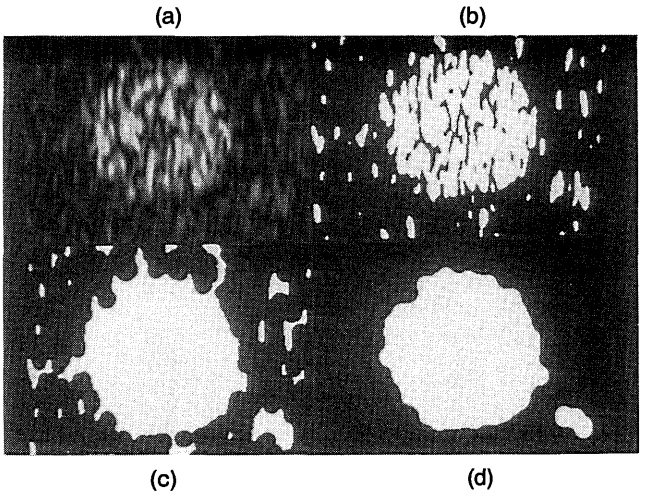

Fig. 1. Example of the segmentation process. (a) Synthetically generated speckle pattern for which the mean of the exterior is 1.0 and the mean of the interior is 3.0. (b) Result of clipping (a) at the maximum-likelihood decision point. (c) Closing of (b) with a circular structuring element of 15 pixels in diameter. (d) Opening of (c) by a circular structuring element of 15 pixels in diameter.

results of the decision rule that may be enumerated as follows:

Case 1: $v \in R_e, d_e$.
Case 2: $v \in R_e, d_i$ (false positive).
Case 3: $v \in R_i, d_i$.
Case 4: $v \in R_i, d_e$ (false negative).

With no loss of generality, assume that $\psi_e < \psi_i$. Then the cases 1 and 3 correspond to a correct decision. Case 4 corresponds to the case for which the envelope faded below the decision level u while in the brighter region R_i. Case 2, on the other hand, corresponds to an excursion of the envelope above the decision level u while in the darker region R_e. The lengths of the fades and excursions are random variables, with well-defined distributions. Therefore we may classify the fades and excursions based on these distributions.

Consider first the case of the fades below the threshold level u. The distribution of the sizes of the fades is dependent on whether the fade is from region R_i or R_e. Using these distributions, we may identify a decision point for classifying the fades based on their sizes. This size threshold can then be implemented by performing the morphological transformation known as a closing on the clipped image of Fig. 1(b). The results of this transformation can be seen in Fig. 1(c). Likewise, each excursion may be classified by using a decision rule based on the size of the excursion as being either from R_e or R_i. The implementation of the size thresholding of the excursions may be performed by the morphological transformation known as an opening. The result of this step is shown in Fig. 1(d). The result is seen to be a suitable segmentation of the image. The details relating to the choice of the maximum-likelihood level for the clipping threshold, the distributions of fade and excursion lengths, the use of the morphological filtering operations of opening and closing for implementing the decision rule on images, and the application of the technique to more complex images having multiple regions and unknown parameters will be addressed in Sections 2–4 of this paper.

2. LEVEL-CROSSING STATISTICS

The random variables related to the events referred to as level crossings are of principal interest to us. These events may be defined as follows.[11]

Let $\xi(t)$ be a continuous real-valued function on the closed interval $[a, b]$, and let u be a real value such that $\xi(t)$ is not identically equal to u in any open interval. Further assume that $\xi(a)$ and $\xi(b)$ are not equal to u.

The function $\xi(t)$ is said to have a crossing of the level u at t_0 if the image of every neighborhood of t_0 contains values both greater than and less than u. Denote the number of crossings in the unit interval as C_u.

The function $\xi(t)$ is said to have an upcrossing of the level u at the point t_0 if there exists an $\epsilon > 0$ such that $\xi(t) \le u$ in $(t_0 - \epsilon, t_0)$ and $\xi(t) \ge u$ in $(t_0, t_0 + \epsilon)$. We shall denote the number of upcrossings in the unit interval as U_u.

The function $\xi(t)$ is said to have a downcrossing of the level u at the point t_0 if there exists an $\epsilon > 0$ such that $\xi(t) \ge u$ in $(t_0 - \epsilon, t_0)$ and $\xi(t) \le u$ in $(t_0, t_0 + \epsilon)$. We shall denote the number of downcrossings in the unit interval as D_u.

The function $\xi(t)$ is said to have a tangency to the level u at the point t_0 if $\xi(t_0) = u$ and is not a crossing of the level u.

In general the tangencies may be ignored since they are events of zero probability. The random variables of interest are the distances between crossings of the level u. An excursion of the envelope below the level u (fade) is the distance from a downcrossing of u to the next upcrossing. Similarly, an excursion of the envelope above the level u (distance between fades) is the distance from an upcrossing of the level u to the next downcrossing. Since the crossings form a stationary stream of events, it follows that the events are independent random variables.

The mean density of the crossings of the level u by a stationary process $\xi(t)$, denoted by $\langle C_u \rangle$, can be expressed in terms of the first-order density of the process $f_\xi(u)$ and the conditional mean of the process derivative $\xi'(t)$ as[12]

$$\langle C_u \rangle = f_\xi(u) \langle |\xi'(t)| \xi(t) = u| \rangle, \tag{4}$$

where $\langle \cdot \rangle$ denotes the expected value of the random variables that it encloses. Since the tangencies are, in general, events of zero probability, it follows that

$$\frac{\langle C_u \rangle}{2} = \langle D_u \rangle = \langle U_u \rangle. \tag{5}$$

The mean length of an excursion is given by[11]

$$\langle x^{\uparrow} | u \rangle = \mu^{-1} \{ P[\xi(0) - v_0(\infty) > u] \}, \tag{6}$$

where $v_k(t) = P[\xi(0) > u, C(0, t) = k]$ and $C(0, t) = k$ denotes the number of crossing in the interval $[0, t]$. When $\xi(t)$ is ergodic, we have $v_0(\infty) = 0$. The expected value of the crossing rate ($= \langle U_u \rangle$) is given by μ. An analogous result holds for the mean length of a fade below the threshold level u:

$$\langle x^{\downarrow} | u \rangle = \mu^{-1} \{ P[\xi(0) - w_0(\infty) < u] \}, \tag{7}$$

where $w_k(t) = P[\xi(0) < u, C(0, t) = k]$.

Many of the results related to level-crossing events involve

the spectral properties of the function being clipped. Let $\xi(t)$ be a stationary process having spectral representation

$$\xi(t) = \int_{-\infty}^{\infty} \exp(jt\lambda)\mathrm{d}\zeta(\lambda). \tag{8}$$

Then the spectral moments are defined as

$$\lambda_n = \int_{-\infty}^{\infty} \lambda^n \mathrm{d}F(\lambda), \tag{9}$$

where $\langle|\mathrm{d}(\zeta)^2 = \mathrm{d}F(\lambda)|\rangle$. In the case when the power spectrum $F(\lambda)$ is absolutely continuous with power spectral density $f(\lambda) = F'(\lambda)$ the Fourier relationship with the autocorrelation results:

$$r(t) = \int_{-\infty}^{\infty} f(\lambda)\exp(jt\lambda)\mathrm{d}\lambda. \tag{10}$$

Thus $|\ddot{r}(0) = \lambda_2|$, and we define $\Delta = \lambda_2 - \lambda_1^2$, a scale factor related to the bandwidth of the system. In the case of ultrasound the relation between speckle size and system parameters is given by Wagner *et al.*[13]

Assume that $\xi(t)$ is a stationary Gaussian process and that λ_2 is finite. The analytic envelope $V(t)$ of $\xi(t)$ has by definition a one-sided power spectrum and a Rayleigh distribution. In the case for which $V(t)$ is an ergodic process, which is the envelope of a zero-mean unit-variance Gaussian stationary process, the expected number of crossings of the level u by the envelope is given by

$$\langle C_u\rangle = \left(\frac{2\Delta}{\pi}\right)^{1/2} u \exp\left(-\frac{u^2}{2}\right). \tag{11}$$

This results in a mean length for a fade below u of

$$\langle x^{\downarrow}|u\rangle = \left(\frac{2\pi}{\Delta}\right)^{1/2} \frac{\exp(u^2/2) - 1}{u} \tag{12}$$

and a mean length of an excursion above u of

$$\langle x^{\uparrow}|u\rangle = \left(\frac{2\pi}{\Delta}\right)^{1/2} \frac{1}{u}. \tag{13}$$

When $\lambda_0 = r(0) \neq 1$ the above result may be modified by making the following replacements:

$$u \rightarrow \frac{u}{(\lambda_0)^{1/2}},$$

$$\Delta \rightarrow \frac{\lambda_0\lambda_2 - \lambda_1^2}{\lambda_0^2}. \tag{14}$$

The expected values of fades and excursions above the threshold level u are displayed in Fig. 2. The following properties of this graph should be noted:

(1) The expected length of the fades is a monotonically increasing function of the clipping level and, for a fixed threshold value, varies inversely as the mean of the process.

(2) The expected length of the excursions is a monotonically decreasing function of the clipping level and, for a fixed threshold value, varies directly as the mean of the process.

The expected values of fades and excursions will be used for normalizing the distance scales in the probability-density functions for the distributions of fades and excursion lengths. While the distributions of fades and excursions are in general quite complex, simple results are easily obtained for the limiting cases when $u \rightarrow 0$ and $u \rightarrow \infty$.[11,14]

Consider first the case of fades as $u \rightarrow \infty$ and the case of excursions when $u \rightarrow 0$. In both of these cases the stationary stream of events asymptotically satisfies the independent increment assumption of a Poisson process. Since the remaining conditions that characterize a Poisson process are satisfied for every stationary stream, it follows that the results for Poisson processes may be directly applied. Therefore the density distribution of the length of the fades approaches the Erlang distribution

$$f^{\downarrow}(\tau, u \rightarrow \infty) = \exp(-\tau), \tag{15}$$

where τ is the length of the fade normalized by the expected length of a fade. Similarly, the length of an excursion above a low level also has an Erlang distribution

$$f^{\uparrow}(\zeta, u \rightarrow 0) = \exp(-\zeta). \tag{16}$$

Here, however, ζ is the length of the excursion normalized by the expected length of an excursion.

The remaining two limiting cases are more complex. Consider first the distribution of fades below the level u as $u \rightarrow 0$. Once again, it is advantageous to normalize the length of the fade by the expected length of the fade. The resulting distribution is given by

$$f^{\downarrow}(\tau, u \rightarrow 0) = 2\pi z^2 \exp(-z)\left[I_0(z) - \left(1 + \frac{1}{2z}\right) I_1(z)\right], \tag{17}$$

where $z = 2/(\pi\tau^2)$ and $I_0(z)$ and $I_1(z)$ are, respectively, the zero- and first-order modified Bessel functions. The case

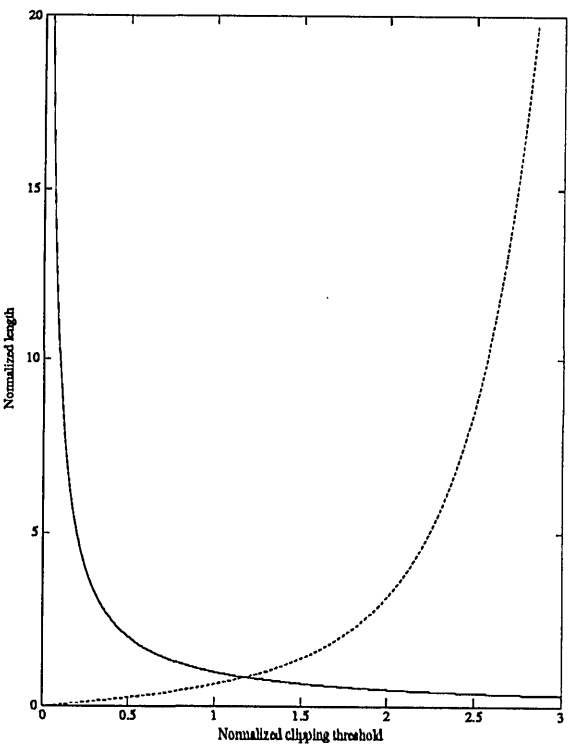

Fig. 2. Mean lengths of fades (dashed curve), the mean length of excursions (solid curve), and the mean distance between fades (excursions) for the envelope of a speckle process.

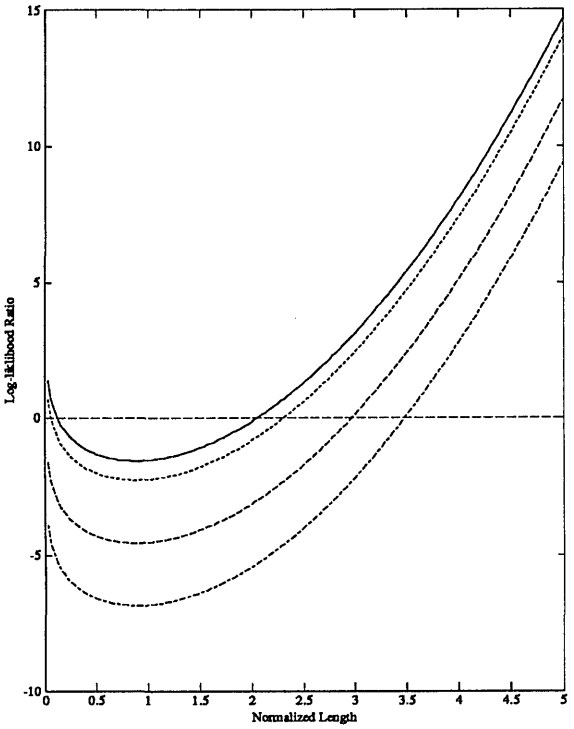

Fig. 3. Log-likelihood ratio of an excursion of normalized length x_1 using the large ratio of means approximation for ratios of 5.0 (solid curve), 10.0 (short-dashed curve), 100.0 (long dashed curve), 1000.0 (dotted–dashed curve).

for the normalized length of an excursion as $u \to \infty$ is given by the Rayleigh distribution

$$f^{\uparrow}(\zeta, u \to \infty) = \frac{\pi}{2}\zeta \exp\left(-\frac{\pi}{4}\zeta^2\right). \tag{18}$$

These distributions are plotted in Fig. 3.

3. SEGMENTATION

The lengths of the fades and excursions are random variables that are independent.[6] We shall consider the classification of fades and excursions as a decision problem. In this case each pixel within a fade or excursion will be classified based on the decision about whether the fade or excursion is from R_1 or R_2. In the example of Section 2 we chose the maximum-likelihood decision point, which has implicitly assumed that we have no *a priori* knowledge with regard to the sizes of the two regions. If we want to retain this assumption when the decision rule is based on the sizes of the fades and excursions in the clipped image, we are forced to use a maximum *a posteriori* (MAP) decision rule; i.e.,

$$\frac{p(z|m_1)}{p(z|m_2)} \underset{d_1}{\overset{d_2}{\lessgtr}} \frac{p(m_2)}{p(m_1)}, \tag{19}$$

where m_1 and m_2 are the events that the random variable z is contained in the regimes R_1 and R_2, respectively. The message probabilities on the right-hand side of the equation reflect the ratios of crossing densities for the two assumed distributions. This is simply the ratio of two Rayleigh distributions. If we choose to clip the image at the maximum-likelihood decision point, then we have the right-hand side of the MAP decision rule going to unity.

Consider the limiting case for which the clipping threshold u is such that $(\psi_1)^{1/2} \ll u \ll \psi_2^{1/2}$. In the limit for the case $u_2 = u/\psi_2^{1/2} \to 0$ the density for the excursions, obtained from Eq. (16), is given by

$$\lim_{u_2 \to 0} f^{\uparrow}(x) = \frac{1}{\bar{x}_2}\exp(-x/\bar{x}_2), \tag{20}$$

where $\bar{x}_2 = \langle x_2^{\uparrow}|u_2\rangle$, while in the case when $u_1 = u/\psi_1^{1/2} \to \infty$ the limiting density is obtained from Eq. (18) and is given by

$$\lim_{u_1 \to \infty} f^{\uparrow}(x) = \frac{\pi}{2}\frac{x}{\bar{x}_1^2}\exp\left[-\frac{\pi}{4}\left(\frac{x}{\bar{x}_1}\right)^2\right], \tag{21}$$

where $\bar{x}_1 = \langle x_1^{\uparrow}|u_1\rangle$. The likelihood function for the excursions in the limiting case of widely separated means is

$$\Lambda_u(x) = \left[\frac{1}{\bar{x}_2}\exp\left(-\frac{x}{\bar{x}_2}\right)\right] \Big/ \left\{\frac{\pi x}{2\bar{x}_1^2}\exp\left[-\frac{\pi}{4}\left(\frac{x}{\bar{x}_1}\right)^2\right]\right\}. \tag{22}$$

We can form the log-likelihood ratio in terms of $x_1 = x/\bar{x}_1$ and $r = (\psi_2/\psi_1)^{1/2}$, getting

$$l_u(x) = \frac{\pi}{4}x_1^2 - \frac{x_1}{r} - \ln(x_1) - \ln\left(\frac{\pi}{2}r\right), \tag{23}$$

where we have made use of Eq. (13) to eliminate terms in $\bar{x}_2$. The log-likelihood ratio for several values of r is displayed in Fig. 3.

The maximum-likelihood test assumes that the ratios of excursions in the two regions are equally likely, thus resulting in the decision rule

$$l_u(x) \underset{d_2}{\overset{d_1}{\lessgtr}} 0. \tag{24}$$

In fact the ratio is strongly dependent on the clipping threshold. For this reason, a MAP decision criterion, i.e.,

$$\frac{P(z|m_1)}{P(z|m_2)} \underset{d_1}{\overset{d_2}{\lessgtr}} \frac{P(m_2)}{P(m_1)}, \tag{25}$$

is a reasonable one. The ratio of the message probabilities of the right-hand side is just the ratio of the crossing rates of the level u given in Eq. (11). The MAP criterion is thus

$$\Lambda_u(x) \underset{d_1}{\overset{d_2}{\lessgtr}} \Lambda(u), \tag{26}$$

where the right-hand side is simply the likelihood ratio of two Rayleigh distributions. Thus the clipping level, which reduces the MAP criterion to a maximum-likelihood criterion, is seen to be the maximum-likelihood decision point for two Rayleigh distributions [Eq. (3)].

In an analogous manner to the excursions, we can derive a decision rule for classifying the fades of the envelope of a speckle process below a fixed threshold in the limiting case. The limiting form of the probability-density function of the length of fades below a low level, obtained from Eq. (17), is given by

$$\lim_{u_2 \to 0} f^{\downarrow}(x) = \frac{1}{\bar{x}_2}2\pi z^2 \exp(-z)\left[I_0(z) - \left(1 + \frac{1}{2z}\right)I_1(z)\right], \tag{27}$$

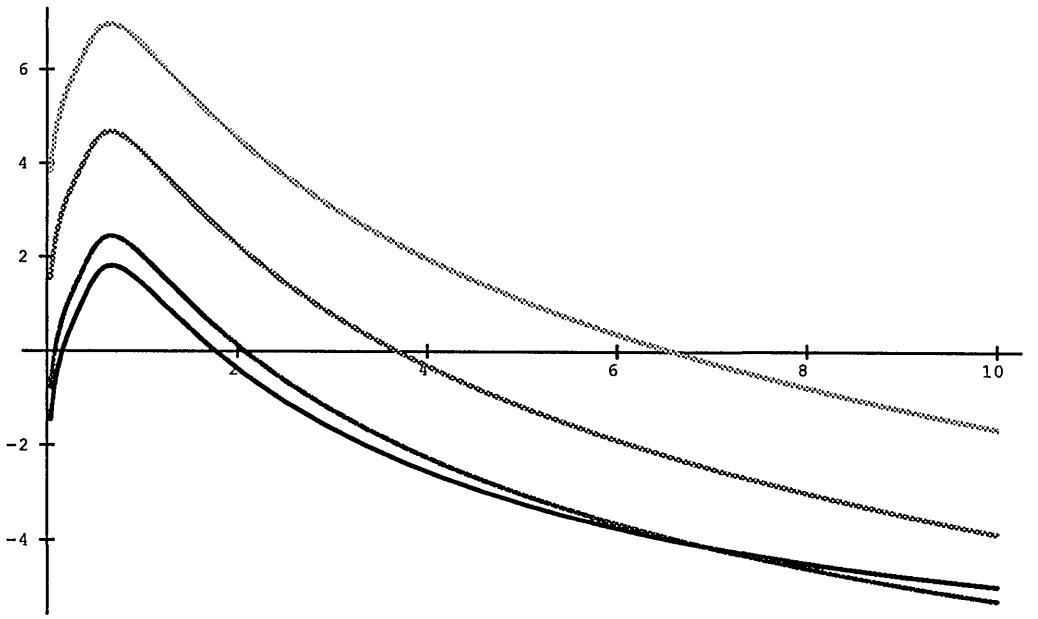

Fig. 4. Log-likelihood ratio for a fade of normalized length x_2 using the large ratios of means approximation for ratios 5.0 (solid curve), 10.0 (short-dashed curve), 100.0 (long dashed curve), 1000.0 (dotted–dashed curve).

where $z = 2\bar{x}_2^2/\pi x^2$ and $\bar{x}_2 = \langle x_2^{\downarrow}|u_2\rangle$. Similarly, the limiting form of the probability-density function of the length of fades below a large level, obtained from Eq. (15), is

$$\lim_{u_1\to\infty} f^{\downarrow}(x) = \frac{1}{\bar{x}_1}\exp\left(-\frac{x}{\bar{x}_1}\right), \tag{28}$$

where $\bar{x}_1 = \langle x_1^{\downarrow}|u_1\rangle$. For the case for which the clipping threshold is set to the maximum-likelihood decision point, the log-likelihood ratio is plotted in Fig. 4 for several values of $r = (\psi_2/\psi_1)^{1/2}$ as a function of $x_2 = x/\bar{x}_2$. A close approximation to the maximum-likelihood decision point may be obtained by noting that

$$\lim_{u_2\to 0} \bar{x}_2 = \left(\frac{2\pi}{\Delta}\right)^{1/2}\frac{u_2}{2} + O(u_2^3) \tag{29}$$

and that the term in brackets in Eq. (17) asymptotically approaches 3/4 for small values of z. Therefore

$$\lim_{u_2\to 0} f^{\downarrow}(x) = \frac{1}{\bar{x}_2}\frac{6}{\pi}\frac{\bar{x}_2^4}{x^4}\exp\left(-\frac{2\bar{x}_2^2}{\pi x^2}\right). \tag{30}$$

The likelihood function for the fades in the limiting case of widely separated means $u_2 \ll x$ is given by

$$\Lambda_u^{\downarrow}(x) = \left[\frac{1}{\bar{x}_2}\frac{6}{\pi}\frac{\bar{x}_2^4}{x^4}\exp\left(-\frac{2\bar{x}_2^2}{\pi x^2}\right)\right]\Bigg/\left[\frac{1}{\bar{x}_1}\exp\left(-\frac{x}{\bar{x}_1}\right)\right]. \tag{31}$$

As in the previous case for the excursions, we can express the log-likelihood ratio as a function of $x_2 = x/\bar{x}_2$,

$$l_u^{\downarrow}(x) = \ln\left(\frac{6\bar{x}_1}{\pi\bar{x}_2}\right) - 4\ln(x_2) - \frac{2}{\pi x_2^2} + \frac{x}{\bar{x}_1}. \tag{32}$$

Since the clipping is at the maximum-likelihood decision point, we have

$$\bar{x}_1 = \left(\frac{2\pi}{\Delta}\right)^{1/2}\left\{\exp\left[\frac{2\ln(r)}{1-r}\right] - 1\right\}\Bigg/\left[\frac{2\ln(r)}{1-r}\right]^{1/2}. \tag{33}$$

When we are dealing with the nonlimiting case, closed-form solutions for the distribution functions are not known; however, numerical solutions are possible.[5,14] These solutions show that the shape of the normalized distribution undergoes a gradual transition between the limiting cases. It is therefore the normalization factor that predominates in the case of the nonnormalized distributions on which the decisions are based.

4. SIZE MEASUREMENT

Mathematical morphology provides a framework in which a collection of geometric filtering techniques has been formalized.[15] The results were initially used in stochastic geometry for the measurement of the size of random sets. Our principal interests are not far removed from this initial use. The problem that we face is the measurement of the sizes of random sets created by clipping speckle images. In this section we shall present a brief introduction to the terminology and mathematical formalism and shall show how these techniques may be applied to the image segmentation problem.

An image may be represented as a function mapping an m-dimensional Euclidean space into the real line. In the case of clipped images, the domain space is two dimensional, and the range is restricted to the set {0, 1}. Such a function will be referred to as a binary image. In the following definitions, the sets $\mathcal{A}$ and $\mathcal{B}$ are subsets of Euclidean vector space. The translation of the set $\mathcal{A}$ by the vector $\mathbf{x} \in \mathcal{B}$ is denoted as

$$\mathcal{A}_{\mathbf{x}} = \mathcal{A} + \mathbf{x} = \{\mathbf{y} + \mathbf{x} | \mathbf{y} \in \mathcal{A}\}. \tag{34}$$

The scalar multiplication of $\mathcal{A}$ by the scalar $\mathbf{c}$ is denoted as

$$\mathbf{c}\mathcal{A} = \{\mathbf{c} \cdot \mathbf{x} | \mathbf{x} \in \mathcal{A}\}. \tag{35}$$

The reflection of $\mathcal{A}$ is the special case

$$\check{\mathcal{A}} = -\mathcal{A} = \{-\mathbf{x} | \mathbf{x} \in \mathcal{A}\}. \tag{36}$$

Clearly if $\mathcal{A}$ is symmetric, then $\mathcal{A} = \check{\mathcal{A}}$.

The Minkowski sum of $\mathcal{A}$ and $\mathcal{B}$ is defined as

$$\mathcal{A} \oplus \mathcal{B} = \{\mathbf{x} + \mathbf{y} | \mathbf{x} \in \mathcal{A}, \mathbf{y} \in \mathcal{B}\}. \tag{37}$$

It is easily shown that

$$\mathcal{A} \oplus \mathcal{B} = \bigcup_{\mathbf{y} \in \mathcal{B}} \mathcal{A}_{\mathbf{y}} = \bigcup_{\mathbf{x} \in \mathcal{A}} \mathcal{B}_{\mathbf{x}}. \tag{38}$$

The dilation of $\mathcal{A}$ by $\mathcal{B}$ is defined as the Minkowski sum $\mathcal{A} \oplus \check{\mathcal{B}}$. The effect of a Minkowski sum or a dilation of a set $\mathcal{A}$ by a compact set $\mathcal{B}$ is to extend the boundaries of $\mathcal{A}$, filling in cavities. The set theoretic dual to the Minkowski addition, the Minkowski difference, is defined as

$$\mathcal{A} \ominus \mathcal{B} = \bigcap_{\mathbf{y} \in \mathcal{B}} \mathcal{A}_{\mathbf{y}}, \tag{39}$$

and the erosion of $\mathcal{A}$ by $\mathcal{B}$ is defined as the Minkowski difference $\mathcal{A} \ominus \check{\mathcal{B}}$. The effect of a Minkowski subtraction or erosion is to shrink the boundaries of $\mathcal{A}$, producing smaller fragments or eliminating them altogether.

An opening of a set $\mathcal{A}$ by a set $\mathcal{B}$ is defined as

$$\mathcal{A}_{\mathcal{B}} = (\mathcal{A} \ominus \check{\mathcal{B}}) \oplus \mathcal{B} \tag{40}$$

or, from Eqs. (39) and (38), as

$$\mathcal{A}_{\mathcal{B}} = \bigcup_{\mathbf{x} \in \mathcal{B}} \bigcap_{\mathbf{y} \in \mathcal{B}} \mathcal{A}_{\mathbf{x}-\mathbf{y}}, \tag{41}$$

which is the union of all the translates of $\mathcal{B}$ that are contained in $\mathcal{A}$. While the closing of $\mathcal{A}$ by $\mathcal{B}$ is the set theoretic dual defined as

$$\mathcal{A}^{\mathcal{B}} = (\mathcal{A} \oplus \check{\mathcal{B}}) \ominus \mathcal{B} \tag{42}$$

or, once again from Eqs. (39) and (38), as

$$\mathcal{A}_{\mathcal{B}} = \bigcap_{\mathbf{x} \in \mathcal{B}} \bigcup_{\mathbf{y} \in \mathcal{B}} \mathcal{A}_{\mathbf{x}-\mathbf{y}}, \tag{43}$$

which is the union of all the translates of $\mathcal{B}$ that are contained in the complement of $\mathcal{A}$, i.e., the opening of the complement of $\mathcal{A}$.

In morphological filtering the set $\mathcal{A}$ usually denotes the set formed from the image, and the set $\mathcal{B}$, usually much smaller than $\mathcal{A}$, is referred to as a structuring element.

In our context, that of the segmentation of speckle, the structuring element will be chosen to have the basic shape and size of the postulated speckle distributions. Thus the level-crossing analysis can be quickly implemented by using the morphological closing and opening operations.

5. RESULTS

The results of Sections 2–4 may be applied to the simple case for which we have an image composed of two speckle regions having known parameters. For this purpose, software was written to generate synthetic speckle images with known parameters and contents. These images were constructed by generating independent, zero-mean, white, unit-variance, complex circular Gaussian variates that multiply some mean-value pixels in a given image. The resulting image, which models random scatterers of varying amplitude, is then convolved with a two-dimensional function whose parameters were chosen to match the parameters of an acoustic pulse generated by a typical clinical B-scan instrument. These parameters result in a Gaussian envelope in the range direction having a standard deviation of 7.2 pixels. The envelope in the transverse direction is of the form

$$\left[\frac{J_1(x)^2}{x}\right], \tag{44}$$

where $J_1(x)$ is a first-order Bessel function and x has been scaled so that the first zero occurs at 6.7 pixels. The resulting waveforms are envelopes detected to produce the desired speckle images.

The structuring element was constructed from the basic two-dimensional pulse shape, with the scale factor of $(2\pi/\Delta)^{1/2}$ in Eqs. (12) and (13) taken as 7.2 pixels in the range direction and 2.9 in transverse direction. A boundary of two times the basic structuring element was eliminated before the statistics in each region were computed.

The results presented are for a two-region segmentation both with and without *a priori* knowledge of the means of the regions. The results appearing in Figs. 5–7 and Tables 1–3 (operations using *a priori* known means) show that a significant improvement in the segmentation of speckle images can be obtained with the use of clipping and morphological filtering, as opposed to the use of clipping alone. The improvement is most evident in the cases for which the ratio of the means is in excess of 3 or less than 1/3. In these cases nearly all the fades and excursions that contribute to the errors in the region segmentation are identified and removed. The tabulated results show the number of pixels placed into each region, the arithmetic mean in each region, and the mean divided by the standard deviation in each region. The size of the circular region is 128 pixels in diameter. If the transition between the regions is assumed to occur at the point where the expected value is halfway between the means of the two regions, the number of pixels interior to the circle is 12,868, and 52,668 pixels are exterior to it. In the estimates pixels on the boundary were removed by dilating each of the identified regions by using a structuring element 2 standard deviations in size and forming the intersection of the two resulting sets. In the ideal case this reduces the number of pixels in the interior region to ~10,923 pixels and the exterior region to ~50,591 pixels. The method of boundary identification used here tends to overestimate the size of the boundary, so in general the observed sizes of the two regions will be smaller than in the ideal case.

While the arithmetic estimate of the mean intensity is unbiased, the estimators for the variance of the intensity are only asymptotically unbiased. Hence, in the case for which the number of speckle spots contained in a region is small, the estimate of the ratio of the mean to the standard deviation will be high.[16] In the results appearing in Figs. 5–7 and Tables 1–3 the segmented regions are sufficiently large to

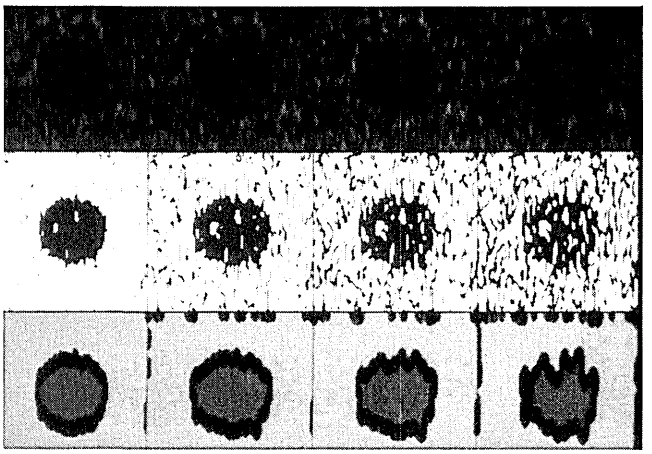

(a) (b) (c) (d)

Fig. 5. Segmentation of a 256 × 256-pixel synthetic speckle image with a circle of 128 pixels in diameter. The top row is the image displayed with a logarithmic palette. The center row is the result of thresholding at the maximum-likelihood decision point. The bottom row displays the result of the segmentation algorithm with known means. The columns from left to right have means of (a) 10–100, (b) 20–100, (c) 30–100, (d) 40–100.

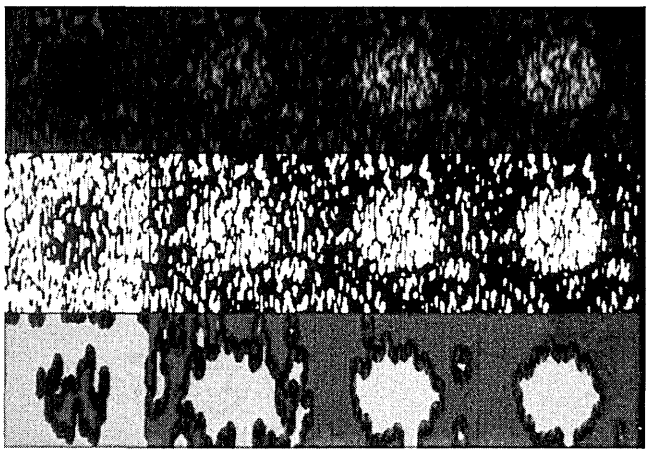

(a) (b) (c) (d)

Fig. 6. Same as Fig. 5 for known means with ratios of (a) 50:100, (b) 150:100, (c) 200:100, (d) 250:100.

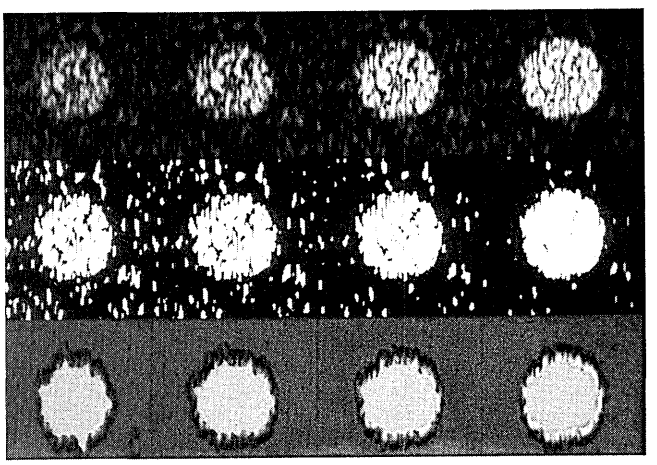

(a) (b) (c) (d)

Fig. 7. Same as Fig. 5 for known means with ratios of (a) 300:100, (b) 350:100, (c) 500:100, (d) 1000:100.

result in a negligibly biased ratio of the mean to the standard deviation. For similar regions Wear and Popp[16] and Tuthill *et al.*[9] obtained values of 1.91 ± 0.1, which is in agreement with the values that were obtained in our results.

For comparative purposes, the images in Figs. 5–7 were generated by using an identical seed value for the random-number generator. This resulted in a speckle pattern having an average value of 106.1 instead of the theoretically expected mean of 100. In Figs. 5–7 we see the effect of clipping the images at the maximum-likelihood decision point, as determined from the parameters supplied to simulation software. Also shown is the result of the opening and the closing operations together with the boundary elimination.

Figure 8 and Table 4 display the ability of the algorithm to identify regions as a function of size. For comparative purposes the same initial seeds were used in each figure; howev-

Table 1. Statistics Resulting from the Segmentation of the Images in Fig. 5[a]

Figure	Threshold	*N*	Mean	Mean/SD
5(a)	24	6473	11.4	1.92
		48663	105.5	1.87
5(b)	41	6897	23.1	1.99
		45545	106.4	1.89
5(c)	55	6759	34.7	1.98
		45794	106.1	1.89
5(d)	67	5072	45.6	1.90
		42022	105.3	1.88

[a] SD, standard deviation.

Table 2. Statistics Resulting from the Segmentation of the Images in Fig. 6[a]

Figure	Threshold	*N*	Mean	Mean/SD
6(a)	77	1776	51.1	1.99
		43890	104.3	1.87
6(b)	136	16360	151.7	1.87
		13556	85.3	1.80
6(c)	153	11164	221.3	1.96
		37776	100.9	1.84
6(d)	167	10519	282.8	1.99
		43680	102.3	1.85

[a] SD, standard deviation.

Table 3. Statistics Resulting from the Segmentation of the Images in Fig. 7[a]

Figure	Threshold	*N*	Mean	Mean/SD
7(a)	177	10416	340.9	2.00
		44338	102.3	1.86
7(b)	186	9900	404.8	2.03
		46438	103.7	1.85
7(c)	207	9804	583.7	2.06
		46670	104.1	1.85
7(d)	243	10381	1162.1	2.07
		42022	104.1	1.85

[a] SD, standard deviation.

er, the seeds were changed between columns. In the case for which the means of the two regions are known, the algorithm is insensitive to the number of fades and excursions that make up a region. In the case for which the means are unknown, however, the size of the region influences the ability to estimate the means of the two regions correctly, and the results of the segmentation degrade accordingly.

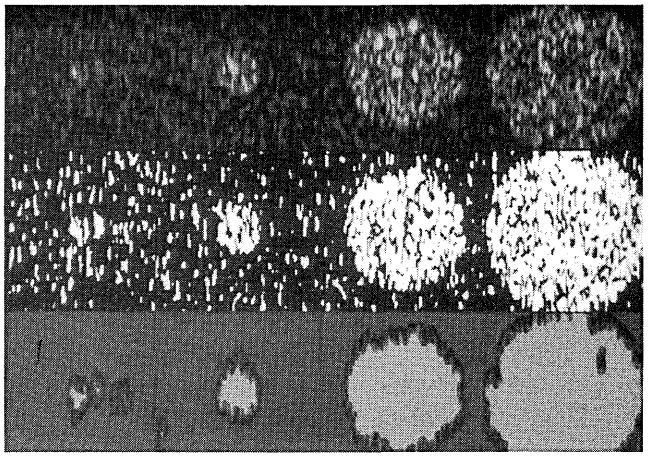

(a) (b) (c) (d)

Fig. 8. Circles of mean 300 in a background of 100 with diameters of (a) 32 pixels, (b) 64 pixels, (c) 182 pixels, (d) 256 pixels. The threshold was set to the maximum likelihood by using the known parameters.

Table 4. Statistics Resulting from the Segmentation of the Images in Fig. 8[a]

Figure	Threshold	N	Mean	Mean/SD
8(a)	177	371	275.0	1.79
		59367	106.3	1.89
8(b)	177	2238	313.5	1.87
		57202	102.1	1.94
8(c)	177	21424	315.9	1.77
		30786	99.6	1.97
8(d)	177	43607	305.2	1.87
		7343	108.2	2.07

[a] SD, standard deviation.

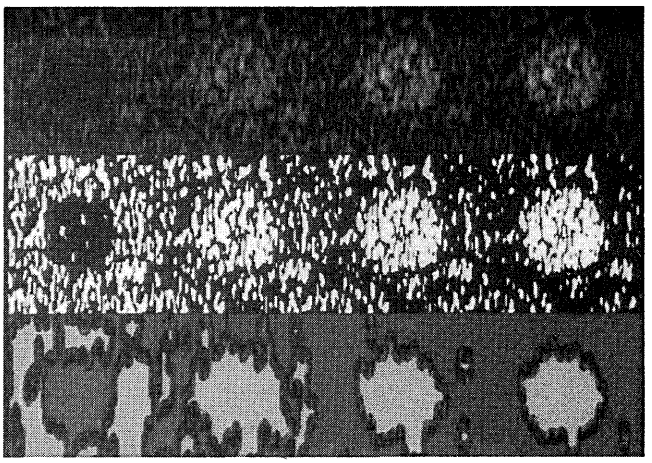

(a) (b) (c) (d)

Fig. 9. Same as Fig. 5 for unknown means with ratios of (a) 50:100, (b) 150:100, (c) 200:100, (d) 250:100.

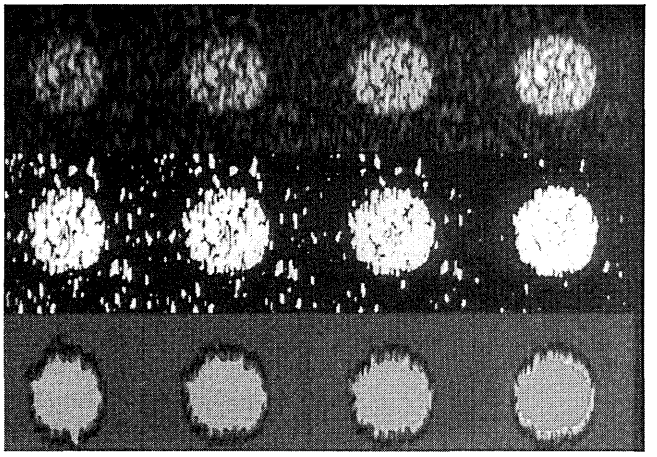

(a) (b) (c) (d)

Fig. 10. Same as Fig. 5 for unknown means with ratios of (a) 300:100, (b) 350:100, (c) 500:100, (d) 1000:100.

Figures 9 and 10 show the same cases analyzed in Figs. 6 and 7 except that the algorithm is no longer supplied with *a priori* known means. In these cases conventional statistical tests are employed first to test the postulate that the image is derived from a single mean Rayleigh process (or exponential probability density distribution) if intensities are analyzed.[8] If this postulate is rejected, then an estimate of the maximum-likelihood decision point is obtained, and the process continues with thresholding and morphological filtering.[8] The results in Figs. 9 and 10 are similar to those for the previous cases in which known means were entered. This shows that the overall approach is robust and can be applied to segmentation of speckle images in the practical situation for which mean values are not known *a priori*.

6. CONCLUSIONS

We have shown how fully developed speckle images may be segmented based on the statistical properties of their level crossings. This method shows promise for the identification of homogeneous regions in speckle contaminated images. The monotonicity of the expected values of fades and excursions allows us to split an image recursively when several regions are present. Further, the parameters themselves may be estimated from these procedures.

ACKNOWLEDGMENTS

This research was supported by National Institutes of Health grant CA44732 and by the Department of Electrical Engineering, University of Rochester, Rochester, New York.

R. H. Sperry is currently with Systems Integration Incorporated, P.O. Box 63051, Rochester, New York 14623.

REFERENCES

1. J. W. Goodman, "Statistical properties of laser speckle patterns," in *Laser Speckle and Related Phenomena*, J. C. Dainty, ed. (Springer-Verlag, Berlin, 1975), pp. 9–75.
2. D. Middleton, *An Introduction to Statistical Communications Theory* (McGraw-Hill, New York, 1960).
3. J. Marron and G. M. Morris, "Properties of clipped laser speckle," in *Speckle*, H. H. Arsenault, ed., Proc. Soc. Photo-Opt. Instrum. Eng. **556**, 39–44 (1985).
4. R. Barakat, "Clipped photon-counting covariance functions," J. Opt. Soc. Am. A **5**, 1248–1253 (1988).
5. S. O. Rice, "Distribution of the durations of fades in radio transmission: Gaussian noise model," Bell Syst. Tech. J. **27**, 581–635 (1958).
6. R. Barakat, "Level-crossing statistics of aperature integrated speckle," J. Opt. Soc. Am. A **5**, 1244–1247 (1988).
7. K. J. Parker, "Attenuation measurement uncertainties caused by speckle statistics," J. Acoust. Soc. Am. **80**, 727–734 (1986).
8. R. H. Sperry, "Segmentation of speckle images based on level crossing statistics," Ph.D. dissertation (University of Rochester, Rochester, N.Y., 1989).
9. T. A. Tuthill, R. H. Sperry, and K. J. Parker, "Deviations from Rayleigh statistics in ultrasound speckle," Ultrasonic Imag. **10**, 81–89 (1988).
10. J. L. Melsa and D. L. Cohen, *Decision and Estimation Theory* (McGraw-Hill, New York, 1978).
11. H. Cramer and M. R. Leadbetter, *Stationary and Related Stochastic Processes* (Wiley, New York, 1967).
12. A. Papoulis, *Probability, Random Variables and Stochastic Processes* (McGraw-Hill, New York, 1984).
13. R. F. Wagner, M. F. Insana, and D. G. Brown, "Statistical properties of radio-frequency and envelope-detected signals with applications to medical ultrasound," J. Opt. Soc. Am. A **4**, 910–922 (1987).
14. A. J. Rainal, "Duration of fades associated with radar clutter," Bell Syst. Tech. J. **45**, 1285–1298 (1966).
15. J. Serra, *Image Analysis and Mathematical Morphology* (Academic, London, 1982).
16. K. A. Wear and R. L. Popp, "Methods for estimation of statistical properties of envelopes of ultrasonic echoes from myocardium," IEEE Trans. Med. Imag. **MI-6**, 281–291 (1987).